Rate Control Management of Atrial Fibrillation: May a Mathematical Model Suggest an Ideal Heart Rate?

Attosecond-controlled photoemission from metal nanowire tips in the few-electron regime

Cite as: APL Photonics **2**, 036104 (2017); https://doi.org/10.1063/1.4974529
Submitted: 24 October 2016 . Accepted: 10 January 2017 . Published Online: 07 February 2017

B. Ahn, J. Schötz, M. Kang, W. A. Okell, S. Mitra, B. Förg, S. Zherebtsov, F. Süßmann, C. Burger, M. Kübel, C. Liu, A. Wirth, E. Di Fabrizio, H. Yanagisawa, D. Kim, B. Kim, and M. F. Kling

APL PHOTONICS **2**, 036104 (2017)

Attosecond-controlled photoemission from metal nanowire tips in the few-electron regime

B. Ahn,[1,2,3] J. Schötz,[3,4] M. Kang,[5,6] W. A. Okell,[3] S. Mitra,[3] B. Förg,[3,4] S. Zherebtsov,[3,4] F. Süßmann,[3,4] C. Burger,[3,4] M. Kübel,[3,4] C. Liu,[3] A. Wirth,[3] E. Di Fabrizio,[7] H. Yanagisawa,[3] D. Kim,[1,2,a] B. Kim,[5,a] and M. F. Kling[1,3,4,a]
[1]*Physics Department, POSTECH, Pohang, Gyeongbuk 376-73, South Korea*
[2]*Max Planck Center for Attosecond Science, Pohang, Gyeongbuk 376-73, South Korea*
[3]*Max Planck Institute of Quantum Optics, D-85748 Garching, Germany*
[4]*Physics Department, Ludwig-Maximilians-Universität München, D-85748 Garching, Germany*
[5]*Department of Chemistry, KAIST, Daejeon 305-701, South Korea*
[6]*BioNanotechnoloy Research Center, KRIBB, Daejeon 305-806, South Korea*
[7]*King Abdullah University of Science and Technology, Thuwal, Saudi Arabia*

(Received 24 October 2016; accepted 10 January 2017; published online 7 February 2017)

Metal nanotip photoemitters have proven to be versatile in fundamental nanoplasmonics research and applications, including, e.g., the generation of ultrafast electron pulses, the adiabatic focusing of plasmons, and as light-triggered electron sources for microscopy. Here, we report the generation of high energy photoelectrons (up to 160 eV) in photoemission from single-crystalline nanowire tips in few-cycle, 750-nm laser fields at peak intensities of (2-7.3) $\times 10^{12}$ W/cm^2. Recording the carrier-envelope phase (CEP)-dependent photoemission from the nanowire tips allows us to identify rescattering contributions and also permits us to determine the high-energy cutoff of the electron spectra as a function of laser intensity. So far these types of experiments from metal nanotips have been limited to an emission regime with less than one electron per pulse. We detect up to 13 *e*/shot and given the limited detection efficiency, we expect up to a few ten times more electrons being emitted from the nanowire. Within the investigated intensity range, we find linear scaling of cutoff energies. The nonlinear scaling of electron count rates is consistent with tunneling photoemission occurring in the absence of significant charge interaction. The high electron energy gain is attributed to field-induced rescattering in the enhanced nanolocalized fields at the wires apex, where a strong CEP-modulation is indicative of the attosecond control of photoemission. [http://dx.doi.org/10.1063/1.4974529]

I. INTRODUCTION

The progress in the field of nanophotonics has been fueled by advances in fabrication techniques such as lithography[1,2] and chemical synthesis,[3] where optical properties of nanomaterials are used to achieve functionality.[4,5] Collective electron motion as a result of the interaction of ultrashort light pulses with nanomaterials typically unfolds on attosecond to femtosecond time scales, where its properties depend on the waveform of the laser field,[6] and the material, composition,[7] shape,[8] and configuration[2] of nanomaterials, and their local environment.[9,10] Strong external fields may even induce a nonlinear behavior and transitions in electronic properties of nanomaterials on ultrafast time scales.[11–15] The many applications arising within the field of nanophotonics motivate a more detailed understanding of collective electron dynamics. While spectroscopic methods give only limited information about dynamical processes, time-resolved measurements performed on the time scale of the

[a]Authors to whom correspondence should be addressed. Electronic addresses: kimd@postech.ac.kr; nanobio@kaist.ac.kr; and matthias.kling@lmu.de.

fastest dynamics are extremely powerful in order to gain much deeper insight into the underlying fundamental processes and have the potential to disentangle the complex multi-electron physics.[16]

The photoemission from metal nanotips is of particular interest offering the possibility to produce ultrashort electron pulses. These in turn can be used to seed electron accelerators,[17,18] and as an electron source for transmission[19] and diffraction imaging studies,[1] offering Angstrom spatial and down to attosecond temporal resolutions. It was recently found that the electron emission from metallic nanotips can be controlled with the carrier-envelope phase (CEP) of few-cycle laser pulses in the single-electron emission regime.[20,21] The field-control of matter waves also opens up possibilities to use such structures in ultrafast electronics applications.[14] Along this line, laser-driven nanotip vacuum-diodes[22] have been demonstrated.

In our present study, we investigate the carrier-envelope phase control of the photoemission from single-crystalline Au nanowires, which have been prepared by vapor transport method and mounted on tungsten tips. The wires have a large aspect ratio with a typical thickness of 90-190 nm and a length of tens of micrometers. They furthermore exhibit crystal edges at their apex in contrast to etched wires, which typically have a rounded apex. Our studies demonstrate that photoelectrons from nanowires can be strongly accelerated in the local near-fields reaching up to 160 eV in an intensity range of (2-7.3) $\times$ 10^{12} W/cm^2. We detect several electrons per laser shot. Our experiments cover the range between previous CEP-resolved photoemission experiments on metal nanotips[20,21] (single-electron regime) and on nanospheres[23,24] (many-electron regime), where in the latter case the electron dynamics is strongly dominated by the interaction between electrons and between ions and electrons. Charge interaction effects in CEP-resolved photoemission have also been studied theoretically for metal nanotips.[21] We investigate the impact of charge interaction on the intensity dependence of the electron count rate, the kinetic energy cutoff, and the CEP-resolved spectra. Irrespective of multi-electron emission from the nanowire tips at these intensities, we find a strong CEP-dependence for the range of rescattering electrons, indicative of the attosecond control of electron emission.[20,25]

II. APPROACH

A. Experimental setup

In the experiments, few-cycle near-infrared laser pulses are used to initiate photoemission from a chemically prepared gold nanowire tip. Photoelectron kinetic energies are measured as a function of CEP and laser intensity. A schematic of the experimental setup is shown in Fig. 1(a). The laser system consists of a Ti:sapphire oscillator (Femtolasers Rainbow), which is CEP-stabilized in a feed-forward-scheme after the oscillator.[26] The pulses from the oscillator are temporally stretched in a prism stretcher and used to seed the multi-pass amplifier (Femtopower HR, 10 kHz, CEP4) that produces 20 fs, 800 μJ laser pulses at a repetition rate of 10 kHz. A 1-m long, 250 μm inner diameter hollow core glass fiber filled with 3 bars of Ne gas is used for spectral broadening through self-phase modulation followed by temporal compression with a series of negatively chirped mirrors to a pulse duration of 4.5 fs (full-width-at-half-maximum of the intensity envelope). The laser spectrum is centered at 750 nm and extends from 500 nm to 1000 nm (1% level of intensity). The carrier-envelope phase (CEP) of the few-cycle pulses is monitored by an f-2f-interferometer. A feedback to one of the prisms in the prism-stretcher is provided to correct for slow-drifts of the CEP. Inside the experimental vacuum chamber, the few-cycle pulses are focused onto the apex of the tip using a near-normal incidence spherical mirror with 10 cm focal length to a spot size of approximately 15 μm. The work function of a single crystalline gold is typically around 5 eV.[27–30] For the few-cycle laser pulse with a photon energy of 1.65 eV, at least four photons are needed to eject an electron into the continuum. The laser intensity is varied using a variable neutral density (ND) filter, where scanning the variable ND filter does not produce a detectable change in pulse duration or CEP. For each setting of the ND filter, the laser pulse energy is measured. Calibration of the energy to intensity conversion is performed at the highest intensity from a measurement on argon gas. The polarization is aligned parallel to the nanowire axis and parallel to the axis of a time-of-flight (TOF) electron spectrometer (e-TOF, Kaesdorf GmbH). Electrons are detected on a chevron microchannel-plate (MCP). The signals from the MCP are further amplified and counted with a digital multi-channel

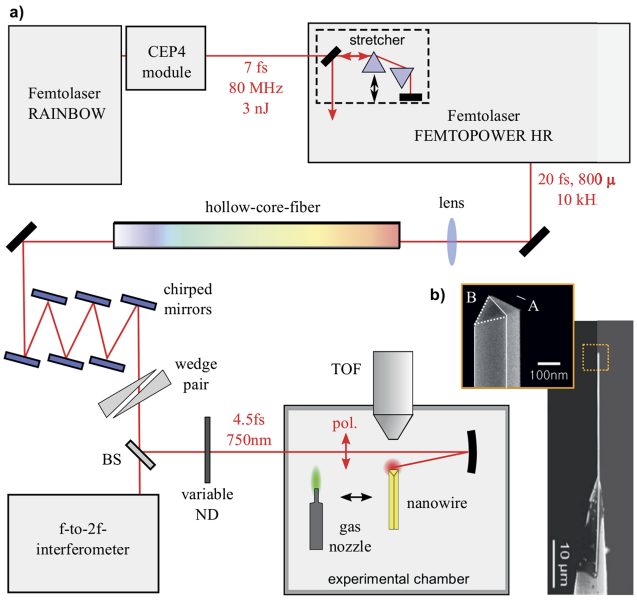

FIG. 1. (a) Schematic of the experimental setup. The laser system generates 20 fs pulses that are spectrally broadened in a gas-filled hollow-core fiber (HCF) and temporally compressed to 4.5 fs with a series of multilayer chirped mirrors (CMs). The 4.5 fs pulses are focused onto the gold nano-wire tip in the experimental chamber and photoelectrons are detected using a time-of-flight spectrometer (TOF). For laser intensity calibration, a gas nozzle is used. (b) Scanning electron microscope (SEM) images of the gold nanowire tip on its tungsten tip support.

scaler (P7889, FAST Comtec) with 100 ps resolution. The energy resolution is energy dependent and monotonically decreasing from 0.1 eV at an electron kinetic energy of 5 eV to ~1.5 eV at 150 eV. The use of a TOF to measure electrons has the advantage that the entire electron spectrum can be recorded simultaneously and also an electron count rate per shot can be determined. During measurements on the nanowire samples, the pressure in the vacuum chamber was typically below 5×10^{-7} mbar.

B. Nanowire tip fabrication

The gold nanowires are grown by epitaxial deposition on a sapphire substrate, achieved by means of simple vapor transport.[31] This allows us to produce Au nanowires with diameters between 90 nm and 190 nm with a well-defined crystalline structure and lengths of about 10 μm–50 μm. The nanowires are mounted free-standing on a tungsten tip (T-4-10, GGB industries, Inc.). Figure 1(b) shows a scanning electron microscope (SEM) image of such a gold nanowire. The gold nanowires are single crystalline without twins or defects and grow along the (110) direction.[32] Each nanowire is an elongated half-octahedron, made up of four side facets, two (111) top facets consisting of equilateral triangular planes, and a (110) bottom surface with the epitaxial relationship between (110) gold nanowires and (0001) sapphire. For the mounting, a sharp tungsten tip mounted on a manipulator is used to approach a gold nanowire vertically grown on a sapphire substrate. By the van der Waals force, the tungsten tip can pick up the nanowire. Prior to picking up the nanowire, the tungsten tip can be coated with conducting adhesives such as Ag paste (Norland Products, Inc.) or carbon paste (CANS) to facilitate high conductivity between the Au wire and W tip. All the nanowires used in our study have been tested to be electrically well contacted to the tungsten tip to avoid charging during the laser irradiation.

III. RESULTS AND DISCUSSION

In order to visualize and quantify the field enhancement at the apex of the nanowire, a series of finite-difference-time-domain (FDTD, Lumerical, version 8.3) simulations were performed. The total simulation region was set to $(2 \times 2 \times 2)$ μm^3. The nanowire tip is surrounded by vacuum (index of refraction $n = 1$) and the real and imaginary parts of the wavelength-dependent dielectric functions of

gold were taken from the work of Johson and Christy.[33] A perfectly matched layer boundary condition with a thickness of 1.2 μm is applied to minimize reflections of outgoing fields at the boundary of the simulation region. The angles between the facets of the nanowire are modeled by taking into account the FCC crystal structure of gold. The distance AB (Fig. 2(a)) was chosen to be 150 nm and the radius of curvature at the transition of the different facets was taken to be 10 nm, estimated from SEM-pictures. The laser beam is modeled as a Gaussian beam with the wave vector parallel to the y-axis and the polarization parallel to the z-axis (tip shaft) with a duration of 4.5 fs (intensity-FWHM) and a central wavelength of 750 nm. The results for the maximum field strength of the component parallel to the nanowire axis normalized by the incident field strength are shown in Fig. 2. The field enhancement depends on the orientation of the ridge of the nanowire to the laser propagation direction. Two scenarios are depicted in Fig. 2 with the ridge on the apex being aligned perpendicular (a) and parallel (b) to the laser propagation direction. From simulations it can be observed that the maximum field enhancement is along the ridge of the nanowire. Additionally, the two rounded corners A and

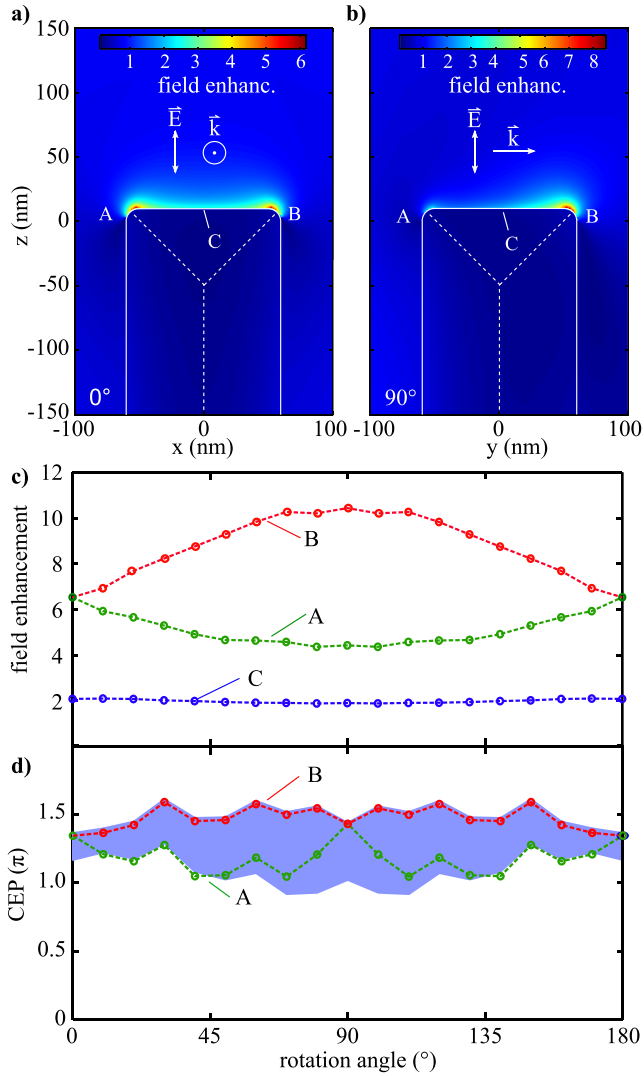

FIG. 2. ((a) and (b)) Electric field distributions in the vicinity of a nanowire's apex for two different orientations where the ridge is oriented perpendicular (a) or parallel (b) to the laser propagation direction. The white solid and dashed lines sketch the geometry of the nanowire used in simulations [compare SEM-image in Fig. 1(b)]. (c) Field enhancement as a function of the rotation angle at the rounded corners A and B on the nanowire apex, as well as the minimum field enhancement along the ridge C. (d) Carrier-envelope phase at the points of maximum field enhancement (dashed lines) as well as the range of minimum and maximum CEP along the ridge (blue area).

B terminating the nanowire (see Fig. 1(b)) act as poles of maximum field enhancement. When the nanowire is rotated around its axis with respect to the propagation direction, the field enhancement on the rounded corners changes as shown in Fig. 2(c). The maximum field enhancement is found on the corner B (red open circles) and varies between ~6.6 for a rotation angle of 0° and ~10.4 for 90°. On the other corner A (green open circles), the enhancement decreases to ~4.4. It can be observed that the field enhancement varies considerably along the ridge. In order to illustrate the range of the variation, the minimum field enhancement is shown as blue dashed line in Fig. 2(c). The location of the minimum enhancement (C) is always close to the middle of the ridge. Additionally, the CEP of the local electric field transients as a function of rotation angle was examined relative to an input pulse with CEP = 0. In Fig. 2(d) the CEP at the point of maximum field enhancement at both rounded corners A (green) and B (red) is shown, as well as the range of maximum and minimum CEP along the ridge (blue area). Generally, a shift of the CEP of around 0.7 π can be observed. Furthermore, there is a spread of CEP phases, which increases from 0.2 π at a rotation angle of 0° to 0.6 π at an angle of 80°. This means that compared to strong-field photoemission experiments in gases and also from edged nanotips,[11,34,35] the strong-field emitted electrons will experience a considerable range of different local field strengths as well as CEPs. We also checked different radii of the transition of the individual facets of 5 and 15 nm for parallel (perpendicular) orientation, which resulted in maximum field enhancements of ~8.5 (~5) and ~14 (~8.5), respectively.

We can extract a few more general trends from the FDTD simulations. The field enhancement rises with decreasing tip radius, as can be expected from geometrical arguments.[36,37] In contrast to conical metal nanotips, the nanowire can exhibit a rather large field enhancement because of its crystal termination at the apex, which in principle allows much smaller radii, potentially down close to the single-atom scale. Experimentally it proved difficult to rotate the nanowire *in situ* in the experiments while keeping the alignment of the wire with respect to the laser focus. In our first results presented here, the orientation of the apex of the wires is unknown; hence, maximum field enhancement factors between ~5 and ~14 can be expected.

Photoelectron kinetic energy spectra were obtained from the TOF measurements and are recorded as a function of intensity and CEP of the few-cycle pulses. The photoelectron spectra as a function of laser intensity are shown in Fig. 3(a). Electrons of very high kinetic energy up to 160 eV are detected for a laser intensity of only 7.3×10^{12} W/cm^2. A strong low energy peak and a plateau at higher energies that become more prominent with increasing intensities can be observed. In contrast to similar studies on etched tungsten nanotips[20] and our experiments in argon, we do not observe individual photon peaks. Furthermore, the rescattering plateau is less pronounced. This could be attributed to the combined effect of the averaging over different emission sites and consequently different field strengths as discussed above, and different initial states as well as multiple electron emission. A number of recent studies[38–41] have focused on the excitations of electrons inside the metal and their influence on photoemission. For the low-repetition rate in our experiment,[38] the short laser pulse duration,[40] and the large tip volume compared to etched tips with the same radius,[41] we do

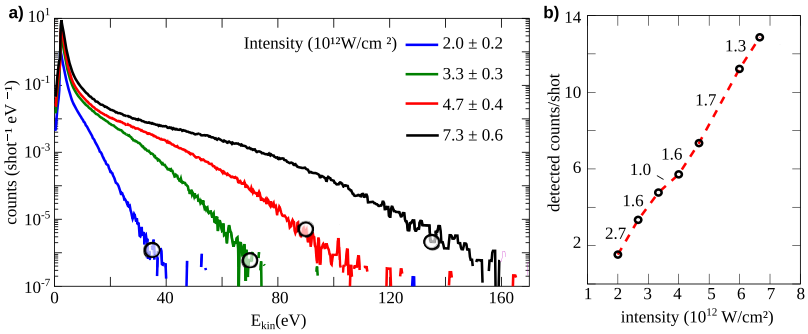

FIG. 3. (a) Photoelectron kinetic energy spectra (CEP averaged) taken from a gold nanowire as a function of incident laser intensity. The cutoff energies are indicated by open circles. Their determination is described in the text. (b) Scaling of the detected counts per shot as a function of laser intensity (note the linear scales). The numbers next to the dashed red line indicate the order of nonlinearity of the count rate increase between two data points.

not expect to observe a significant contribution of this effect. The data do not provide clear signatures of thermionic emission; however, we expect future dedicated experimental and theoretical studies to shed some more light on this topic.

Figure 3(b) shows the number of detected electrons per shot, ranging from slightly below 2 at a laser intensity of 1.9×10^{12} W/cm^2 up to 13 at 7.3×10^{12} W/cm^2. Given the small acceptance angle of around 6° as well as the limited detection efficiency of the microchannel plate detector of the TOF spectrometer, we estimate the number of emitted electrons to be a factor of 10 to 100 higher. Especially at higher input intensities, we therefore might expect to observe evidence for the charge-interaction of emitted electrons. The increase of the total number of detected electrons is around 1.0-1.7, as indicated by the numbers next to the dashed line in Fig. 3(b), which show the order of nonlinearity of the count rate scaling between two data points. Experiments performed on etched gold nanotips have reported a similar scaling of the total count rate for intensities above a local intensity above 2-3 $\times 10^{13}$ W/cm^2, which was identified as the onset of the tunneling regime.[35] The Keldysh parameter $\gamma = \sqrt{W_f/(2\,U_p)}$, where W_f is the work function and U_p the ponderomotive potential of the electron motion in the laser field, is used to distinguish between the multiphoton regime ($\gamma > 1$) and the tunneling regime ($\gamma < 1$). Assuming a field enhancement factor of about 6, based on the numerical calculation presented in Fig. 2, we can estimate a local field intensity of about 7×10^{13} W/cm^2 and a Keldysh parameter $\gamma < 1$ already for the lowest employed intensities. This suggests that the experiments are performed in the tunneling regime, consistent with the observed nonlinearities. No clear indication of an effect of charge interaction is observed for the count rate scaling, despite the relatively large amount of emitted electrons from within a small area. It has been argued that the suppression of electron-electron-interactions as compared to flat surfaces is due to the curved surface of the nanotarget and the resulting diverging electron trajectories.[35] Our result is in agreement with experiments on silicon nanotip-arrays.[25] The effect of space-charge on the count rate scaling is expected to be observable only at even higher count rates.

Despite the high dynamic range of the photoelectron spectra, it was difficult to determine the cutoff energy from a change in the slope of the spectra in the cutoff region as, e.g., done in Refs. 20 and 23. The different shape of the spectra might be due to the charge interaction. Additionally, electrons experience different local field enhancements, depending on where they are born on the ridge, resulting in a smearing of the spectra. We thus determined the cutoff energy by a different approach which was already successfully implemented for the photoemission from isolated nanoparticles.[23] An asymmetry in the emission direction of the electrons as a function of CEP can be determined from the spectra as follows:

$$A(E_{kin}, CEP) = \frac{S(E_{kin}, CEP) - S(E_{kin}, CEP + \pi)}{S(E_{kin}, CEP) + S(E_{kin}, CEP + \pi) + \varepsilon}, \tag{1}$$

where the parameter $A(E_{kin}$, CEP) is a function of the kinetic energy and the CEP, S refers to a particular energy spectrum at a specific CEP, and ϵ is a small number to avoid division by zero. Intuitively, the asymmetry parameter measures the relative deviation of the electron yield at a specific energy and CEP from its counterpart that is shifted in phase by π.

The CEP-dependent asymmetries from the nanowire for the four laser intensities shown in Fig. 3(a) are depicted in Figs. 4(a)–4(d). It can be seen that the high energy electrons yield the largest asymmetry amplitudes for each investigated intensity. This is typical for a rescattering process,[20,23] where electrons are first emitted but then driven back to the wire and further accelerated by the field, acquiring high kinetic energies. In the case of atoms, the cutoff for rescattered electrons is found as[42]

$$E_{cutoff} = 10.007 U_P + 0.538 I_P, \tag{2}$$

where U_p is the ponderomotive potential and I_p the ionization potential of the atom which can be replaced by the work function in the case of solids.[11,34] In inhomogeneous fields at nanostructures, electrons might experience the decay of the near-field during their sub-cycle propagation,[43–45] which leads to the suppression of rescattering and a decrease of the cutoff energy compared to Eq. (2). This effect can be characterized by the adiabaticity parameter, the ratio of decay length and quiver amplitude of electron motion.[44] For our experimental parameters (decay length ~10 nm, quiver amplitude <1.5 nm), we obtain adiabaticity parameters between 7 and 14, which is in a regime where

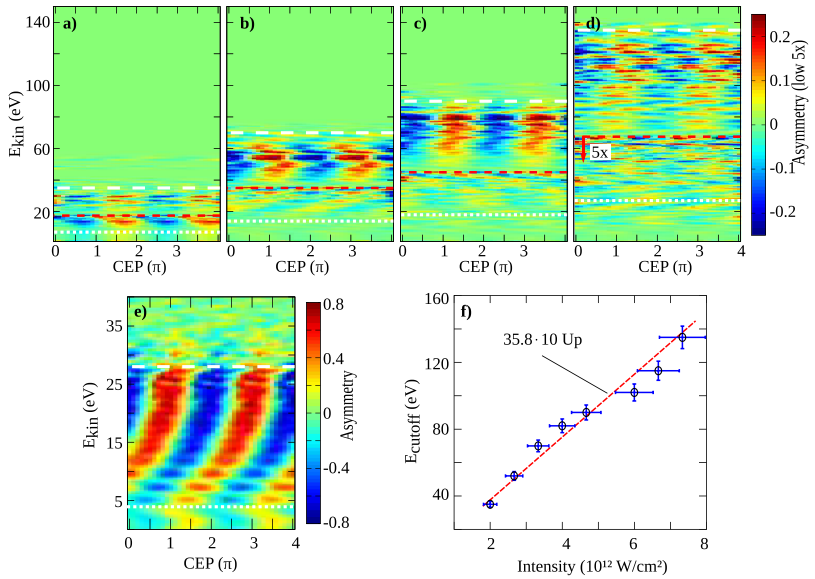

FIG. 4. ((a)-(d)) CEP-dependent asymmetries from the nanowire for the four laser intensities shown in Fig. 3(a). The dashed white line indicates the experimentally determined 10 U_p cutoff from the vanishing asymmetry and the dotted white line the calculated 2 U_p cutoff. The dashed red line is at half of the cutoff energy. The asymmetry scale below the red line is magnified by a factor of 5 relative to the asymmetry scale shown to the right. (e) CEP-dependent asymmetry for electron emission from argon at 3.8×10^{13} W/cm^2 used for calibrating the incident laser intensities. (f) Scaling of the electron cutoff energy with intensity. The dashed red line is a linear fit to the data.

Eq. (2) is valid to a very good approximation. We have also recorded CEP-dependent asymmetries for electron emission from argon, which are shown in Fig. 4(e). These data help in determining the experimental laser intensity (and thus U_p) in the interaction region. For argon, with I_p = 15.8 eV and a cutoff at 28 eV, the intensity is retrieved as 3.8×10^{13} W/cm^2. Calibration of the absolute CEP is required and can also be performed with the argon data since only a relative CEP is obtained from the f-2f measurements. In all cases (for the gas and the nanowires), the asymmetry ceases when the number of field-driven electrons approaches the background noise in the kinetic energy spectra. This point (i.e., where the asymmetry approaches zero at the high-energy end of the spectrum) is taken as the cutoff. The evolution of the cutoff with input intensity for the nanowire measurements is depicted in Fig. 4(f). A linear increase of the cutoff energy with intensity can be seen (as depicted by the linear fit shown as the dashed red line). This behavior is expected for the case, where charge interaction effects can either be neglected or contribute a constant enhancement factor to the cutoffs, similar to what has been observed for the photoemission from nanoparticles.[46] Following this argument, we can define a relation between the experimentally observed cutoff and the incident laser intensity as follows:

$$E_{cutoff} = 10.007 \times \alpha^2 \times b \times U_P + 0.538 W_f, \tag{3}$$

where α is the near-field enhancement factor and b is a factor accounting for the charge interaction. The overall enhancement factor for the field corresponds to $b \times \alpha$ and the overall intensity enhancement to b $\times \alpha^2$, which can be determined from the data to be 35.8. Neglecting charge interaction for a moment, we obtain a field enhancement factor of 5.98 ± 0.24 from the slope in Fig. 4(f), which is in good agreement with the lower estimations of the expected field enhancement from the numerical simulations of the electric field and therefore $b \approx 1$, indicating that the charge interaction does not strongly affect the cutoff energy in the few-electron regime. This is in agreement with experiments on plasmonic nanofilms[47] but different from results for the multi-electron emission from nanoparticles, where charge interaction leads to an extension of the cutoff to higher energies and additionally, as discussed below, a suppression of the low-energy peak in the electron kinetic energy spectrum.[23,24]

The asymmetry data also allow us to obtain information about the electron dynamics. In the gas measurements in Fig. 4(e), the transition between the spectral regions dominated by direct and by

rescattered electrons can be observed by the change of the slope of the asymmetry at a kinetic energy of 2 U_p (indicated by the dotted white line). For the spectral region of direct electrons below 2 U_p, the slope is tilted to the left, while for rescattered electrons, it is tilted to the right. Furthermore, the amplitude of the asymmetry is lower in the spectral region below 2 U_p. The high asymmetry in the cutoff region indicates that electrons with this kinetic energy are created almost exclusively during the central half-cycle of pulses with a certain CEP. By changing the CEP, the electron signal in that region can be switched on ($A \sim 1$) and off ($A \sim -1$). This implies that these electrons are emitted within a fraction of a half-cycle, which amounts to a few 100 as Ref. 20.

From the asymmetry data from the nanowire shown in Figs. 4(a)–4(d), we try to draw similar conclusions on the electron dynamics. In the low energy region, there is no strong asymmetry and only towards the cutoff an increased asymmetry sets in. The asymmetry scale in the spectral region below half of the cutoff energy (red dashed line) is increased by a factor of 5 to enhance the visibility of the asymmetry. For the lower intensities ((a)-(c)), a transition to slightly increased asymmetries at 2 U_p is observable, indicative of rescattering electrons. We attribute the decreased asymmetry in the lower spectral region to the averaging over different field strength and CEPs as discussed above, while the small asymmetry signal is likely to originate from the region of highest intensity. The shape of the asymmetry of the rescattered electrons changes with increasing intensity. For the lowest intensity, it is quasi-straight (a) and then shows a right tilt similar to the gas measurements, which, however, reverses close to the cutoff (b). For higher intensities (c), two regions can be distinguished, at lower and at higher energy, which are quasi-straight and show a relative phase shift of π. This is similar to simulations in the multi-electron regime (see supplementary material of Ref. 21), where a similar structure was observed and explained by the charge interaction of electrons within one bunch and two bunches, respectively, depending on the CEP. We note that the simulations were performed in the sub-cycle emission regime, which requires careful comparison to our experiments. For higher intensities (d) the asymmetry is almost straight and might indicate the transition to the regime studied in Ref. 23. In the cutoff region for all intensities, a strong asymmetry is observed, indicating attosecond control of photoemission in the few-electron regime similar to the gas discussed above.

We note that our observations are slightly different to what has been seen in photoemission from dielectric nanoparticles.[23,24,46] There, the electron emission leads to the creation of a positive charge localized at the surface, creating a trapping potential from which direct electrons cannot escape due to their low kinetic energy. Consequently, direct electrons are completely suppressed and there is a relatively clear asymmetry also at lower kinetic energies. In the electron emission from metals, the electron's parent hole is screened by the other electrons and emitted electrons interact only with their image charge. Whether this might explain the observed differences of the low-energy photoemission has to be clarified in future theoretical studies, which are beyond the scope of the paper. Nevertheless, in agreement with other studies,[21,23,35] our findings indicate that CEP-dependence of the kinetic energy spectrum is possibly more sensitive to charge interaction effects than purely scalar observables as the count rate scaling or cutoff progression. Future experiments could focus on the coherence of the emitted electrons, where we expect the largest and earliest impact of electron-electron interaction.

IV. CONCLUSIONS

We investigated the photoemission from chemically prepared, single-crystalline Au nanowires allowing us to gain insight into the photoemission and acceleration of electrons on attosecond time scales in strong few-cycle fields. We found that the scaling of both the cutoff energies and electron count rates with intensity is consistent with strong-field photoemission in the single-electron regime, despite the emission of multiple electrons from the nanowire tip per laser shot. Charge interaction effects might be found in the details of the CEP-dependence of the electron spectra. The recorded CEP-dependent electron emission asymmetries are indicative of the presence of rescattered electrons and the attosecond control of photoemission at kinetic energies above 100 eV under conditions where multiple electrons are emitted per laser shot. This will be useful for further development in a number of applications, including, e.g., for ultrafast diffractive imaging.

ACKNOWLEDGMENTS

We thank Peter Hommelhoff for very fruitful discussions and Seungchul Kim for help with the nanowire samples. We are grateful for support by the Max Planck Society and the DFG through LMUexcellent, SPP1840 "QUTIF," and the Cluster of Excellence: "Munich Centre for Advanced Photonics (MAP)." B.F. acknowledges support from Marco Allione and Enzo Di Fabrizio via the King Abdullah University of Science and Technology (KAUST). B.F., S.M., S.Z., M.K., F.S., and M.F.K. acknowledge support from the European Union via the ERC grant ATTOCO (Grant No. 307203). This research has been supported in part by Global Research Laboratory Program (Grant No 2009-00439) and by Max Planck POSTECH/KOREA Research Initiative Program (Grant No 2016K1A4A4A01922028) through the National Research Foundation of Korea (NRF) funded by Ministry of Science, ICT & Future Planning.

[1] M. Müller, V. Kravtsov, A. Paarmann, M. B. Raschke, and R. Ernstorfer, ACS Photonics **3**(4), 611–619 (2016).
[2] A. Weber-Bargioni, A. Schwartzberg, M. Schmidt, B. Harteneck, D. Ogletree, P. Schuck, and S. Cabrini, Nanotechnology **21**(6), 065306 (2010).
[3] M. Rycenga, C. M. Cobley, J. Zeng, W. Li, C. H. Moran, Q. Zhang, D. Qin, and Y. Xia, Chem. Rev. **111**(6), 3669–3712 (2011).
[4] M. A. García, J. Phys. D: Appl. Phys. **44**(28), 283001 (2011).
[5] X. T. Geng, B. J. Chun, J. H. Seo, K. Seo, H. Yoon, D.-E. Kim, Y.-J. Kim, and S. Kim, Nat. Commun. **7**, 10685 (2016).
[6] F. Süßmann and M. F. Kling, Phys. Rev. B **84**(12), 121406 (2011).
[7] J. L. West and N. J. Halas, Annu. Rev. Biomed. Eng. **5**(1), 285–292 (2003).
[8] W. A. Murray and W. L. Barnes, Adv. Mater. **19**(22), 3771–3782 (2007).
[9] J. Homola, S. S. Yee, and G. Gauglitz, Sens. Actuators, B **54**(1), 3–15 (1999).
[10] J. J. Mock, D. R. Smith, and S. Schultz, Nano Lett. **3**(4), 485–491 (2003).
[11] S. Thomas, M. Krüger, M. Förster, M. Schenk, and P. Hommelhoff, Nano Lett. **13**(10), 4790–4794 (2013).
[12] F. Krausz and M. I. Stockman, Nat. Photonics **8**(3), 205–213 (2014).
[13] T. Paasch-Colberg, A. Schiffrin, N. Karpowicz, S. Kruchinin, Ö. Sağlam, S. Keiber, O. Razskazovskaya, S. Mühlbrandt, A. Alnaser, and M. Kübel, Nat. Photonics **8**(3), 214–218 (2014).
[14] A. Schiffrin, T. Paasch-Colberg, N. Karpowicz, V. Apalkov, D. Gerster, S. Mühlbrandt, M. Korbman, J. Reichert, M. Schultze, and S. Holzner, Nature **493**(7430), 70–74 (2013).
[15] M. Durach, A. Rusina, M. F. Kling, and M. I. Stockman, Phys. Rev. Lett. **107**(8), 086602 (2011).
[16] M. I. Stockman, M. F. Kling, U. Kleineberg, and F. Krausz, Nat. Photonics **1**(9), 539–544 (2007).
[17] J. Breuer and P. Hommelhoff, Phys. Rev. Lett. **111**(13), 134803 (2013).
[18] J. McNeur, M. Kozak, D. Ehberger, N. Schönenberger, A. Tafel, A. Li, and P. Hommelhoff, J. Phys. B **49**(3), 034006 (2016).
[19] M. Gulde, S. Schweda, G. Storeck, M. Maiti, H. K. Yu, A. M. Wodtke, S. Schäfer, and C. Ropers, Science **345**(6193), 200 (2014).
[20] M. Krüger, M. Schenk, and P. Hommelhoff, Nature **475**(7354), 78–81 (2011).
[21] B. Piglosiewicz, S. Schmidt, D. J. Park, J. Vogelsang, P. Groß, C. Manzoni, P. Farinello, G. Cerullo, and C. Lienau, Nat. Photonics **8**(1), 37–42 (2014).
[22] T. Higuchi, L. Maisenbacher, A. Liehl, P. Dombi, and P. Hommelhoff, Appl. Phys. Lett. **106**(5), 051109 (2015).
[23] S. Zherebtsov, T. Fennel, J. Plenge, E. Antonsson, I. Znakovskaya, A. Wirth, O. Herrwerth, F. Süßmann, C. Peltz, I. Ahmad, S. A. Trushin, V. Pervak, S. Karsch, M. J. J. Vrakking, B. Langer, C. Graf, M. I. Stockman, F. Krausz, E. Ruhl, and M. F. Kling, Nat. Phys. **7**(8), 656–662 (2011).
[24] F. Süßmann, L. Seiffert, S. Zherebtsov, V. Mondes, J. Stierle, M. Arbeiter, J. Plenge, P. Rupp, C. Peltz, A. Kessel, S. A. Trushin, B. Ahn, D. Kim, C. Graf, E. Rühl, M. F. Kling, and T. Fennel, Nat. Commun. **6**, 7944 (2015).
[25] M. E. Swanwick, P. D. Keathley, A. Fallahi, P. R. Krogen, G. Laurent, J. Moses, F. X. Kärtner, and L. F. Velásquez-García, Nano Lett. **14**(9), 5035–5043 (2014).
[26] F. Lücking, V. Crozatier, N. Forget, A. Assion, and F. Krausz, Opt. Lett. **39**(13), 3884–3887 (2014).
[27] J. Lecoeur, J. Bellier, and C. Koehler, Electrochim. Acta **35**(9), 1383–1392 (1990).
[28] G. Valette, J. Electroanal. Chem. Interfacial Electrochem. **139**(2), 285–301 (1982).
[29] G. Hansson and S. Flodström, Phys. Rev. B **18**(4), 1572 (1978).
[30] H. Potter and J. Blakely, J. Vac. Sci. Technol. **12**(1), 279 (1975).
[31] Z. R. Dai, Z. W. Pan, and Z. L. Wang, Adv. Funct. Mater. **13**(1), 9–24 (2003).
[32] Y. Yoo, K. Seo, S. Han, K. S. Varadwaj, H. Y. Kim, J. H. Ryu, H. M. Lee, J. P. Ahn, H. Ihee, and B. Kim, Nano Lett. **10**(2), 432–438 (2010).
[33] S. M. Teichmann, P. Rácz, M. F. Ciappina, J. A. Pérez-Hernández, A. Thai, J. Fekete, A. Y. Elezzabi, L. Veisz, J. Biegert, and P. Dombi, Sci. Rep. **5**, 7584 (2015).
[34] M. Krüger, S. Thomas, M. Förster, and P. Hommelhoff, J. Phys. B **47**(12), 124022 (2014).
[35] R. Bormann, M. Gulde, A. Weismann, S. Yalunin, and C. Ropers, Phys. Rev. Lett. **105**(14), 147601 (2010).
[36] B. Ahn, J. Schötz, W. Okell, F. Süßmann, B. Förg, S. Kim, M. F. Kling, and D. Kim, Opt. Express **24**(1), 92–101 (2016).
[37] S. Thomas, G. Wachter, C. Lemell, J. Burgdörfer, and P. Hommelhoff, New J. Phys. **17**(6), 063010 (2015).
[38] M. Bionta, S. Weber, I. Blum, J. Mauchain, B. Chatel, and B. Chalopin, New J. Phys. **18**(10), 103010 (2016).
[39] H. Yanagisawa, M. Hengsberger, D. Leuenberger, M. Klöckner, C. Hafner, T. Greber, and J. Osterwalder, Phys. Rev. Lett. **107**(8), 087601 (2011).

[40] M. Pant and L. Ang, Phys. Rev. B **88**(19), 195434 (2013).
[41] G. Herink, L. Wimmer, and C. Ropers, New J. Phys. **16**(12), 123005 (2014).
[42] G. G. Paulus, W. Becker, W. Nicklich, and H. Walther, J. Phys. B: At., Mol. Opt. Phys. **27**(21), L703 (1994).
[43] D. J. Park, B. Piglosiewicz, S. Schmidt, H. Kollmann, M. Mascheck, and C. Lienau, Phys. Rev. Lett. **109**(24), 244803 (2012).
[44] G. Herink, D. Solli, M. Gulde, and C. Ropers, Nature **483**(7388), 190–193 (2012).
[45] K. Echternkamp, G. Herink, S. Yalunin, K. Rademann, S. Schäfer, and C. Ropers, Appl. Phys. B **122**(4), 1–10 (2016).
[46] S. Zherebtsov, F. Süßmann, C. Peltz, J. Plenge, K. J. Betsch, I. Znakovskaya, A. S. Alnaser, N. G. Johnson, M. Kübel, A. Horn, V. Mondes, C. Graf, S. Trushin, A. Azzeer, M. J. J. Vrakking, G. G. Paulus, F. Krausz, E. Rühl, T. Fennel, and M. F. Kling, New J. Phys. **14**, 075010 (2012).
[47] S. M. Teichmann, P. Racz, M. F. Ciappina, J. A. Pérez-Hernández, A. Thai, J. Fekete, A. Y. Elezzabi, L. Veisz, J. Biegert, and P. Dombi, Sci. Rep. **5**, 7584 (2015).